

# Analysis of geosynthetic reinforcement in pile-supported embankments. Part I: 3D plate model

B. M. Jones<sup>1</sup>, R. H. Plaut<sup>2</sup> and G. M. Filz<sup>3</sup>

<sup>1</sup>Department of Civil and Environmental Engineering, Virginia Polytechnic Institute and State University, Blacksburg, VA 24061-0105, USA, Telephone: +1 540 231 7151, Telefax: +1 540 231 7532, E-mail: [bjones13@vt.edu](mailto:bjones13@vt.edu)

<sup>2</sup>Department of Civil and Environmental Engineering, Virginia Polytechnic Institute and State University, Blacksburg, VA 24061-0105, USA, Telephone: +1 540 552 0111, Telefax: +1 540 231 7532, E-mail: [rplaut@vt.edu](mailto:rplaut@vt.edu)

<sup>3</sup>Department of Civil and Environmental Engineering, Virginia Polytechnic Institute and State University, Blacksburg, VA 24061-0105, USA, Telephone: +1 540 231 7151, Telefax: +1 540 231 7532, E-mail: [filz@vt.edu](mailto:filz@vt.edu)

Received 28 April 2008, revised 4 January 2010, accepted 5 January 2010

**ABSTRACT:** Geosynthetic reinforcement over a grid of piles in soft soil can help transfer loads to the piles, and reduce settlements. This first part of a three-part study utilises a three-dimensional thin-plate model of the geosynthetic. The von Kármán theory, which includes the effects of bending and stretching, is used. The geosynthetic layer is represented using a linear stress–strain relationship. Owing to symmetry, a one-eighth triangular section of a square unit cell is considered, and the pile caps have either a square, diamond or circular shape. The soil between the pile caps and the geosynthetic, and the soft soil between the piles, are modelled as linear foundations with specified stiffnesses. The embankment stresses over the piles and over the soft soil are also specified. The numerical procedure involves finite differences and minimisation of the total energy. For two sets of parameter values, the effects of the shape of the pile caps on the displacements, strains and net stress reduction ratio are investigated. Sharp spikes in strain and stress occur at the edges of the pile caps. The second paper in this study adopts a three-dimensional cable-net model of the geosynthetic, and an axisymmetric model is analysed in the final paper.

**KEYWORDS:** Geosynthetics, Pile-supported embankment, Three-dimensional, Thin plate, Finite difference method, Energy minimisation

**REFERENCE:** Jones, B. M., Plaut, R. H. & Filz, G. M. (2010). Analysis of geosynthetic reinforcement in pile-supported embankments. Part I: 3D plate model. *Geosynthetics International*, 17, No. 2, 59–67. [doi: 10.1680/gein.2010.17.2.59]

## 1. INTRODUCTION

Geosynthetic-reinforced, pile-supported embankments provide effective geotechnical foundations for roadways and structures in areas of weak subgrade soils. The system includes a soil bridging layer with one or more embedded layers of geosynthetic reinforcement supported by driven, deep-mixed, or other columnar piles. Figure 1 depicts a cross-section of this type of system. The geosynthetic promotes load transfer within the bridging layer to the piles. This technique is generally used when schedule constraints, right-of-way limitations or differential settlements of adjacent structures preclude preload and surcharge solutions.

Current models of the behaviour of the geosynthetic tend to be simple, and usually do not represent the true three-dimensional nature of the displacements, strains and

stresses. Some of these models are described in Horgan and Sarsby (2002), Love and Milligan (2003), Gangakhedkar (2004), Jenck *et al.* (2005), Smith (2005),

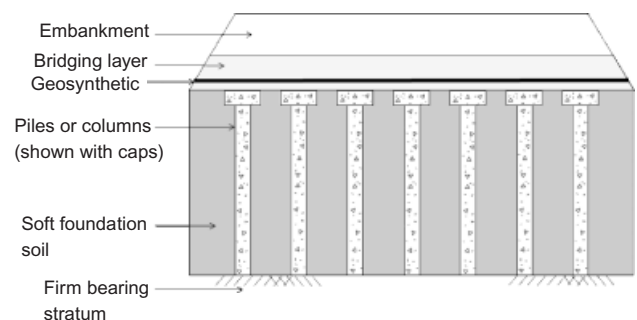


**Figure 1. Cross-section of geosynthetic-reinforced, pile-supported embankment**

Chen and Li (2007), Collin (2007), Oh and Shin (2007), Smith and Filz (2007), Abusharar *et al.* (2008), Chen *et al.* (2008), Gharpure *et al.* (2008), McGuire and Filz (2008), Van Eekelen and Bezuijen (2008), Van Eekelen *et al.* (2008), and the references cited in those studies. Recent additional papers involving geosynthetic-reinforced pile-supported embankments include Camp and Siegel (2006), Abdullah and Edil (2007), Almeida *et al.* (2007), Jenck *et al.* (2007), Liu *et al.* (2007), Zhang *et al.* (2007), Bhandari *et al.* (2009), Filz and Plaut (2009), Han and Bhandari (2009), Huang and Han (2009), Huang *et al.* (2009), McGuire *et al.* (2009) and Zheng *et al.* (2009). A recent book is Kempfert and Gebreselassie (2006).

In Part I of the present investigation, one geosynthetic layer is considered. The geosynthetic is modelled as a thin, flexible, isotropic, homogeneous plate with a linear stress–strain response. The flexural rigidity is very small, and membrane (stretching) behaviour dominates the response. The piles are assumed to be relatively rigid compared with the compressible soil between the piles, and square and circular pile caps are considered.

The foundation system is represented as a distribution of linear springs (i.e. a Winkler foundation), with a high stiffness above the pile caps and a low stiffness elsewhere. Many previous analyses have ignored the support provided to the geosynthetic by the soft underlying soil between pile caps. The embankment stress acting on top of the geosynthetic layer is specified, with a higher value over the pile caps than elsewhere to account for the arching effect in the bridging layer and embankment.

Owing to symmetry, a one-eighth triangular section of the unit cell is analysed. Partial derivatives of the transverse (vertical) and in-plane (horizontal) displacements are approximated by finite differences at a grid of nodes, and the nodal displacements are computed by minimising the total energy of the system. Strains and stress resultants in the geosynthetic are then calculated from the displacements. Spikes in strain and stress occur near the corners of the square and diamond (rotated square) pile caps, and near the edge of the circular piles. Three-dimensional plots are presented to illustrate this feature, and to show the vertical shape of the displaced geosynthetic.

The problem is formulated in Section 2, and the numerical solution procedure is described in Section 3. In Sections 4, 5 and 6, respectively, results are given for square (S), diamond (D), and circular (C) pile-cap configurations for a base case of parameter values. Results for an alternative case are briefly described in Section 7, and concluding remarks are presented in Section 8.

## 2. FORMULATION

This paper considers a grid of piles with the same distance  $L$  between their centres along rows in two perpendicular directions. It is assumed that a unit cell involving four piles can be analysed, owing to symmetry in the system. Figure 2 depicts the three configurations investigated here. Based on the pile-cap shapes, the configurations in Figures 2a, 2b and 2c, respectively, are denoted square

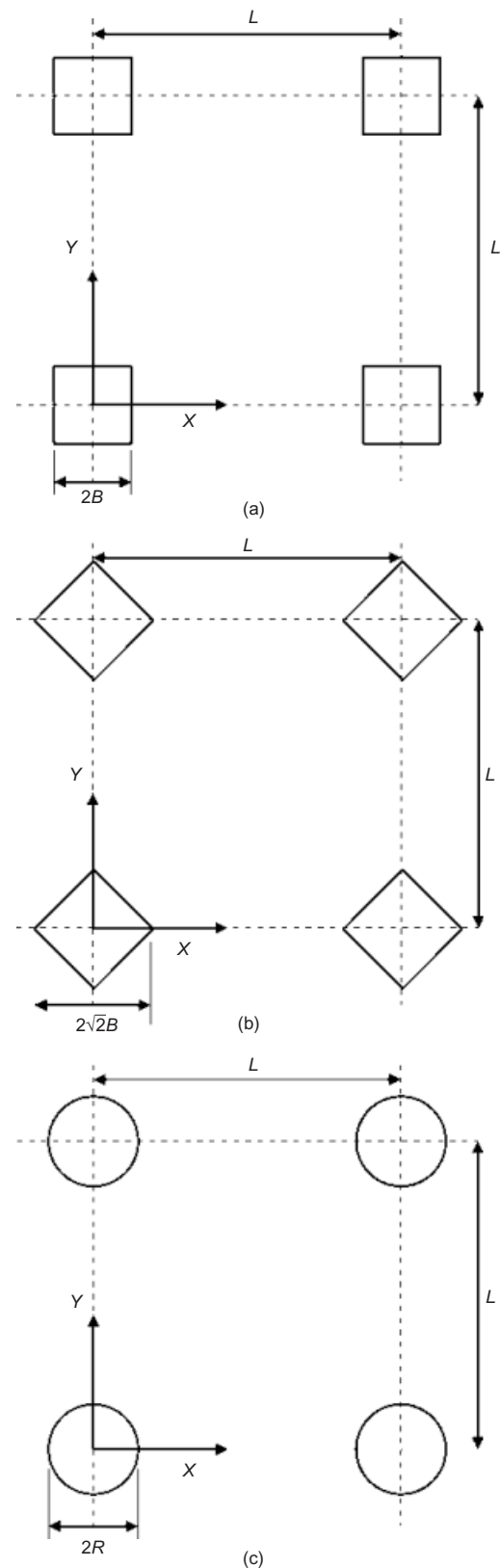


Figure 2. Unit cell: (a) square pile caps (Case S); (b) diamond pile caps (Case D); (c) circular pile caps (Case C)

(S), diamond (D), and circular (C). Consider Figure 2a. The  $X, Y$  coordinate system is shown, with  $0 \leq X \leq L$  and  $0 \leq Y \leq L$  in the unit cell. The square pile caps have width  $2B$ . Figure 3 shows a cross-section through the piles along the  $X$  or  $Y$  axis. The downward stress acting on top

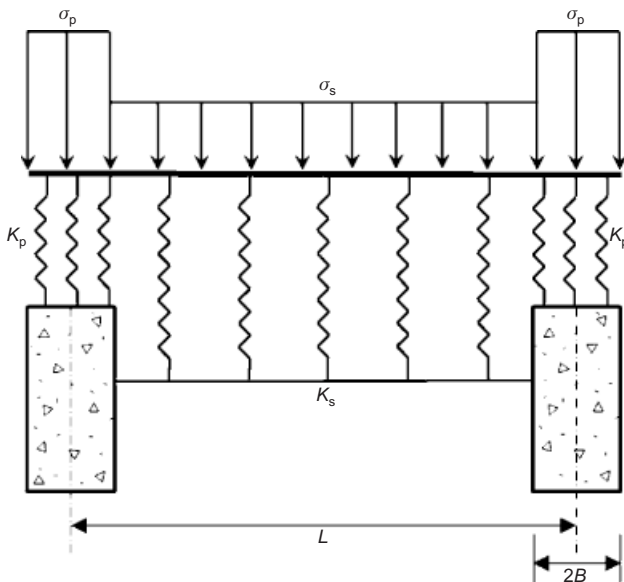


Figure 3. Cross-section along edge of unit cell

of the geosynthetic is  $\sigma_p$  over the pile caps and  $\sigma_s$  over the underlying soft soil. The distributed stiffness of the linear foundation (i.e. the modulus of subgrade reaction) is  $K_p$  under the geosynthetic above the pile caps, and  $K_s$  for the soft soil between pile caps. The stiffness  $K_p$  includes the effect of vertical flexibility of the pile as well as that of the soil between the pile and the geosynthetic layer.

The geosynthetic has no pretension, is assumed to have a linear stress–strain relationship when loaded, and has modulus of elasticity  $E$ , Poisson’s ratio  $\nu$ , thickness  $t$ , and flexural rigidity  $D = Et^3/[12(1 - \nu^2)]$ . As shown in Figure 4, the vertical axis is  $Z$  (positive upwards), the transverse displacement is  $W(X, Y)$ , positive downwards, and the in-plane displacements are  $U(X, Y)$  and  $V(X, Y)$ , positive in the  $X$  and  $Y$  directions, respectively.

The non-linear von Kármán theory is utilised (Timoshenko and Woinowsky-Krieger 1959; Chia 1980; Szilard 2004), which assumes that the strains and the squares of the slopes are small compared with unity. Both bending and stretching effects are included. Owing to symmetry, the in-plane displacements normal to the edges of the unit cell are zero, and stretching of the plate is important in determining displacements, strains, and stress resultants. For the cases to be considered, and other cases involving thin geomembranes and geogrids, the effect of bending is much smaller than the membrane effect.

Non-linear strain-displacement relationships are needed to model the behaviour accurately. Here they are given by

$$\begin{aligned} \epsilon_x &= \frac{\partial U}{\partial X} + \frac{1}{2} \left( \frac{\partial W}{\partial X} \right)^2, \\ \epsilon_y &= \frac{\partial V}{\partial Y} + \frac{1}{2} \left( \frac{\partial W}{\partial Y} \right)^2, \\ \epsilon_{xy} &= \frac{\partial U}{\partial X} + \frac{\partial V}{\partial Y} + \left( \frac{\partial W}{\partial X} \right) \left( \frac{\partial W}{\partial Y} \right) \end{aligned} \quad (1)$$

The relationships between the stress resultants  $N_x, N_y, N_{xy}$  and the strains are given by

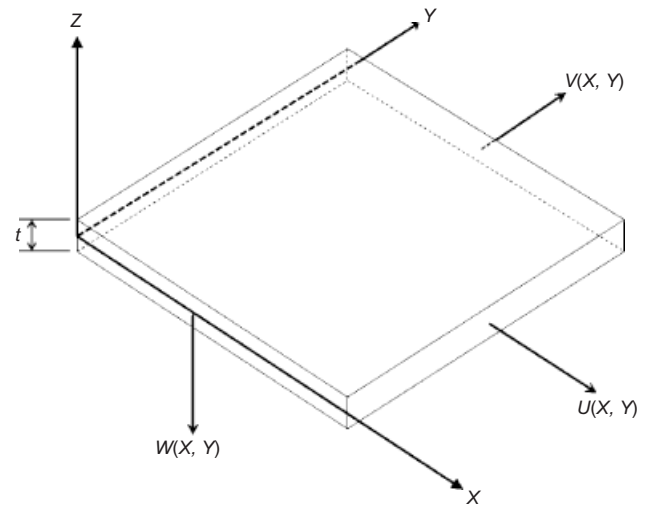


Figure 4. Plate model with axes and displacements

$$\begin{aligned} N_x &= \frac{Et}{1 - \nu^2} (\epsilon_x + \nu \epsilon_y), \\ N_y &= \frac{Et}{1 - \nu^2} (\epsilon_y + \nu \epsilon_x), \\ N_{xy} &= \frac{Et}{2(1 + \nu)} \epsilon_{xy} \end{aligned} \quad (2)$$

The boundary conditions are

$$\begin{aligned} X = 0, L: \quad \frac{\partial W}{\partial X} &= 0, \quad U = 0; \\ Y = 0, L: \quad \frac{\partial W}{\partial Y} &= 0, \quad V = 0 \end{aligned} \quad (3)$$

The total energy  $E_T$  for the unit cell is the sum of: (1) the strain energies  $E_B$  for bending and  $E_M$  for stretching; (2) the stored energy in the soil, denoted  $E_{K_p}$  over the pile caps and  $E_{K_s}$  elsewhere; and (3) the potential energies for the embankment stress, denoted  $E_{\sigma_p}$  over the pile caps and  $E_{\sigma_s}$  elsewhere. These quantities are given by the following equations (Timoshenko and Woinowsky-Krieger 1959; Chia 1980):

$$E_B = \frac{D}{2} \int_0^L \int_0^L \left( \frac{\partial^2 W}{\partial X^2} + \frac{\partial^2 W}{\partial Y^2} \right)^2 dXdY \quad (4)$$

$$\begin{aligned} E_M &= \frac{Et}{2(1 - \nu^2)} \int_0^L \int_0^L \\ &\times \left[ \epsilon_x^2 + \epsilon_y^2 + 2\nu \epsilon_x \epsilon_y + \left( \frac{1 - \nu}{2} \right) \epsilon_{xy}^2 \right] dXdY \end{aligned} \quad (5)$$

$$E_{K_p} = 4 \left( \frac{1}{2} K_p \int_0^B \int_0^B W^2 dXdY \right) \quad (6)$$

$$E_{K_s} = \frac{1}{2} K_s \left( \int_0^L \int_0^L W^2 dXdY - 4 \int_0^B \int_0^B W^2 dXdY \right) \quad (7)$$

$$E_{\sigma_p} = -4\sigma_p \int_0^B \int_0^B W dXdY \quad (8)$$

$$E\sigma_s = -\sigma_s \left( \int_0^L \int_0^L W dXdY - 4 \int_0^B \int_0^B W dXdY \right) \quad (9)$$

The integral limits involving  $B$  are modified for the diamond and circular pile caps (Jones 2007).

### 3. NUMERICAL SOLUTION PROCEDURE

The strains in Equations 1 are substituted into Equation 5. Then the partial derivatives of  $U$ ,  $V$  and  $W$  in the integrands in Equations 4 and 5 are replaced by central differences (e.g. Szilard 2004). The notation

$$\begin{aligned} U_{i,j} &= U(iH, jH), & V_{i,j} &= V(iH, jH), \\ W_{i,j} &= W(iH, jH) \end{aligned} \quad (10)$$

is used.

A triangular section at the bottom left of the unit cell is analysed (e.g. see Figure 1a of Smith and Filz 2007). It comprises one-eighth of the area of the unit cell, and is divided into nodes a distance  $H$  apart parallel to the  $X$  and  $Y$  axes. The number of nodes along an edge of length  $L$  is  $2m+1$ , so that  $H = L/(2m)$ .

In the numerical results to be presented,  $m = 100$  will be used. However, to illustrate the procedure, the case  $m = 5$  is shown in Figure 5. The integrals in Equations 4–9 are approximated as sums over the nodes, with the values of the integrands taken as their values at the node, and these values multiplied by the associated tributary area. Typical tributary areas are shown in Figure 5. For the node at  $(i, j) = (4, 2)$ , the square tributary area is  $H^2$ . At  $(2, 0)$  and  $(2, 2)$ , the area is  $H^2/2$ , at  $(5, 0)$  it is  $H^2/4$ , and at  $(0, 0)$  it is  $H^2/8$ . The nodes in the lower-left portion of the one-eighth section are situated over the pile cap and are involved in the integrals with upper limit  $B$  in Equations 6–9.

Based on symmetry, the general relationships

$$U_{i,j} = V_{j,i}, \quad W_{i,j} = W_{j,i} \quad (11)$$

are used. Along the edges of the one-eighth section, the

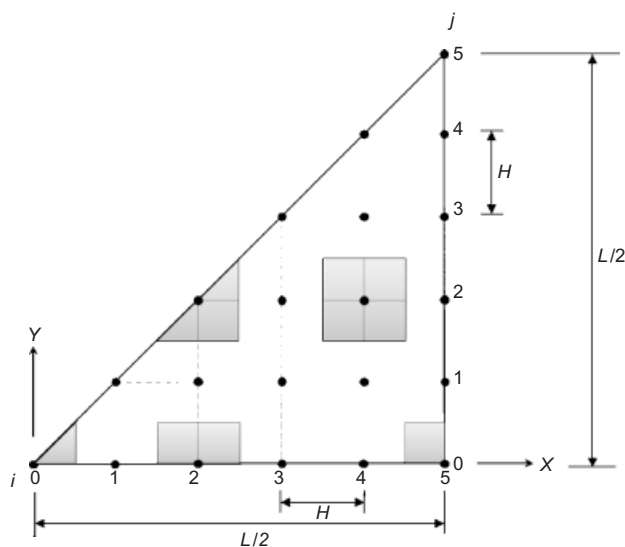


Figure 5. One-eighth section of unit cell with  $m = 5$

finite-difference equations involve displacements outside the section. Symmetry properties are utilised to eliminate those displacements. The relationships in Equations 11 are used along the diagonal edge, and along the other edges they are as follows for  $U$ ,  $V$ , and  $W$ :

$$U_{i,-1} = U_{i,1}, \quad U_{m,j} = 0, \quad U_{m+1,j} = -U_{m-1,j} \quad (12)$$

$$V_{i,0} = 0, \quad V_{i,-1} = -V_{i,1}, \quad V_{m+1,j} = V_{m-1,j} \quad (13)$$

$$W_{i,-1} = W_{i,1}, \quad W_{m+1,j} = W_{m-1,j} \quad (14)$$

The total energy  $E_T$  becomes a function of the nodal displacements  $U_{i,j}$ ,  $V_{i,j}$  and  $W_{i,j}$  in the one-eighth section. Corresponding to equilibrium,  $E_T$  is minimised with respect to these discrete displacements. The computation is conducted using the subroutine FindMinimum in the software package Mathematica (Wolfram 2003). A convergence study determined that the use of  $m = 100$  and an accuracy of seven significant digits is sufficient (e.g. for the base case with square pile caps, the maximum strain was essentially identical for  $m = 70, 80, \dots, 120$ ). Also, the method was verified by comparison with examples in the literature involving clamped plates under uniform pressure (Jones 2007).

The procedure yields nodal displacements for the equilibrium shape of the geosynthetic. Strains and stresses can then be computed using Equations 1 and 2 with finite differences replacing partial derivatives. The numerical calculations are carried out in terms of non-dimensional variables (Jones 2007).

Maximum values of  $W$ ,  $U$  and  $\varepsilon_x$  for Cases S, D, and C are summarised in Table 1, along with the value of the net stress reduction ratio  $SRR_{net}$  (which will be defined at the end of the following section).

### 4. SQUARE PILE CAPS (CASE S)

The values used for the base case with square pile caps (Case S) are as follows:  $B = 0.6$  m,  $L = 3$  m,  $E = 500$  MPa,  $\nu = 0$ ,  $t = 1.5$  mm,  $\sigma_p = 146$  kPa,  $\sigma_s = 30.6$  kPa,  $K_p = 29.2$  MN/m<sup>3</sup>, and  $K_s = 160$  kN/m<sup>3</sup>. Therefore the in-plane stiffness of the geosynthetic is given by  $J = Et = 750$  kN/m. Also, the stress concentration ratio is  $n = \sigma_p / \sigma_s = 4.77$ , the average embankment stress is  $\sigma_{ave} = 49.1$  kPa, and the area replacement ratio is  $a_s = 4B^2 / L^2 = 0.16$ . Since  $\nu = 0$ , the stress resultants  $N_x$  and  $N_y$  are proportional to the strains  $\varepsilon_x$  and  $\varepsilon_y$ , respectively.

The vertical displacement of the geosynthetic in the unit cell is depicted in Figure 6, where the values on the vertical axis are plotted as  $-W$ , so the deflected shape looks like the physical shape of the geosynthetic. The geosynthetic drops sharply at the edges of the pile caps,

Table 1. Maximum values and  $SRR_{net}$  for base case

Case	Max $W$ (cm)	Max $U$ (cm)	Max $\varepsilon_x$	$SRR_{net}$
S	19.1	1.34	0.0395	0.120
D	18.7	1.71	0.0353	0.115
C	19.1	1.35	0.0253	0.110

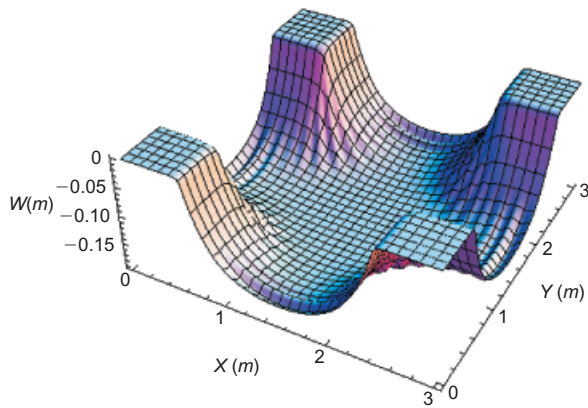


Figure 6. Vertical displacement with square pile caps

and exhibits wrinkles in this region as well as along the edges of the unit cell (i.e. between adjacent piles). The minimum stress resultant is negative where these wrinkles occur.

Figure 7 shows plots of the vertical displacement along the edge  $Y = 0$  (highest curve), the line  $Y = B = 0.6$  m, and the ‘centreline’  $Y = L/2 = 1.5$  m (as well as along similar lines obtained using symmetry). The displacement over the central portion of each pile is essentially constant and equal to the value  $\sigma_p/K_p = 0.5$  cm, which is seen at the ends of the curve for  $Y = 0$ . The maximum downward displacement along the edge is 16.8 cm. For the whole unit cell, the maximum displacement of 19.1 cm occurs at the centre of the plate (i.e. at  $X = Y = 1.5$  m) and has the same value as  $\sigma_s/K_s$ . The central diamond-shaped region with corners at  $(X, Y) = (0.5$  m, 1.5 m), (1.5 m, 0.5 m), (2.5 m, 1.5 m) and (1.5 m, 2.5 m) is almost flat, with downward displacements around 18–19 cm.

In-plane displacements  $U$  parallel to the  $X$  axis are illustrated in Figure 8. They are zero at  $X = 0, L/2,$  and  $L,$  and are linear over the pile caps. The maximum value of  $U$  is 1.34 cm, more than 10 times smaller than the maximum downward displacement. However, the resistance to stretching has a significant influence on  $W$ , and it is important that the bending–stretching coupling is included in the formulation.

Figure 9 depicts a three-dimensional plot of the strain  $\epsilon_x$  over the unit cell. Spikes near the corners of the piles are noteworthy. The maximum value of  $\epsilon_x$  is 0.0395, and hence the maximum value of the stress resultant  $N_x$  is 29.6 kN/m (i.e.  $J$  times the maximum value of  $\epsilon_x$ ).

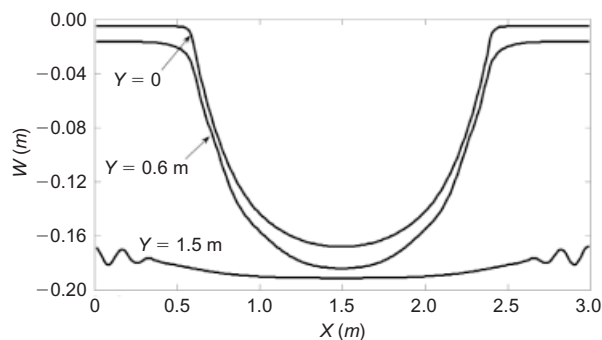


Figure 7. Vertical-displacement profiles with square pile caps

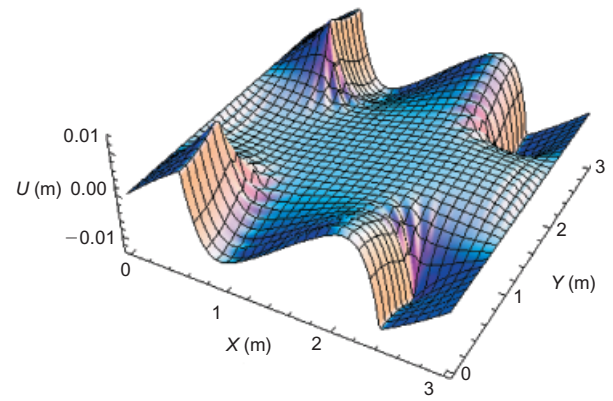


Figure 8. In-plane displacement  $U$  with square pile caps

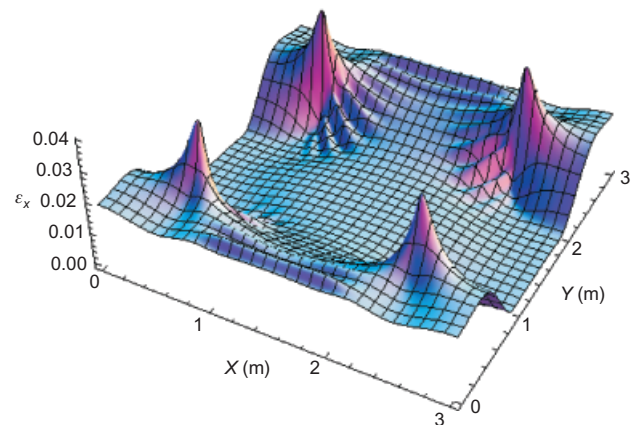


Figure 9. Strain  $\epsilon_x$  with square pile caps

The net stress reduction ratio  $SRR_{net}$  is defined as the ratio of the average net downward stress on the geosynthetic in the area not supported by piles to the average downward stress of the embankment over the unit cell (Smith and Filz 2007). A larger value of  $SRR_{net}$  means that a greater portion of the embankment load is carried by the geosynthetic and less by the underlying compressible soil between the piles. For Case S,  $SRR_{net}$  is given by

$$SRR_{net} = \frac{\sigma_s - \frac{K_s}{L^2 - 4B^2} \left( \int_0^L \int_0^L W \, dX \, dY - 4 \int_0^B \int_0^B W \, dX \, dY \right)}{\sigma_{ave}} \quad (15)$$

Its value is 0.120, as listed in Table 1.

### 5. DIAMOND PILE CAPS (CASE D)

The case in Figure 2b is considered in this section. The pile caps are rotated by  $45^\circ$  from their orientation in Case S. By rotating Figure 2b by  $45^\circ$ , one can also interpret this case as representing square pile caps with staggered rows. All parameter values are the same as in Case S.

A three-dimensional illustration of the vertical displace-

ment is presented in Figure 10. Figure 11 depicts the vertical displacement along the edge  $Y=0$  (highest curve), the line  $Y=1.414B=0.85$  m (with its ends at corners of pile caps), and the centreline  $Y=L/2=1.5$  m. The maximum downward displacement along the edge is 15.5 cm, and the central displacement is 18.7 cm, both of which are smaller than for Case S. The geosynthetic is almost flat in the same diamond-shaped central region as for Case S. The maximum in-plane displacement is 1.71 cm, which is larger than for Case S but still less than 10% of the maximum transverse displacement.

Much less wrinkling occurs in this case. For Case S, wrinkles exist in a significant region around the flat central area of the unit cell and out to the central parts of the edges. For Case D, they exist only in small regions along the central portions of the edges, where Figure 10 shows a little waviness.

The strains exhibit spikes near the corners of the pile caps, which now are situated along the edges of the unit cell. The maximum value of  $\epsilon_x$  is 0.0353, which is smaller than for Case S. The net stress reduction ratio  $SRR_{net}$  is 0.115, slightly smaller than for Case S.

## 6. CIRCULAR PILE CAPS (CASE C)

Now circular pile caps are analysed, as shown in Figure 2c. The radius of the pile cap is chosen as  $R=1.128B$  to give the same area as for the square and diamond pile

caps. Again, the parameter values are the same as in Case S.

Figures 12 and 13 correspond to the previous pairs of figures for the downward displacement, with the middle curve in Figure 13 associated with  $Y=R=0.677$  m. The maximum downward displacement along the edge is 16.1 cm, and the value at the centre is the same as for Case S, 19.1 cm. The flat central diamond-shaped region is slightly larger here than for Cases S and D. The maximum in-plane displacement is 1.35 cm, similar to that in Case S. The region with wrinkles is similar in shape to that in Case S, around the pile caps and along the edges of the unit cell, but it covers a smaller area here.

The spikes in strain are significantly smaller in this case than in Cases S and D, since the pile cap has no corner. The computational procedure led to an erratic picture of the strain spikes around the edge of the pile cap, since the finite difference grid consists of squares and has difficulties representing the behaviour along the circular edge. The maximum value of  $\epsilon_x$  was found to be 0.0253, i.e. 36% lower than that for Case S and 28% lower than that for Case D. The largest value of  $N_{max}$  is 19.5 kN/m. The net stress reduction ratio  $SRR_{net}$  for the circular piles is 0.110, i.e. 8% lower than for Case S and 4% lower than for Case D.

Further consideration of circular piles will be presented in Part III (Plaut and Filz 2010), where an axisymmetric analysis is carried out and the incompatibility of a square grid with a circular edge is avoided.

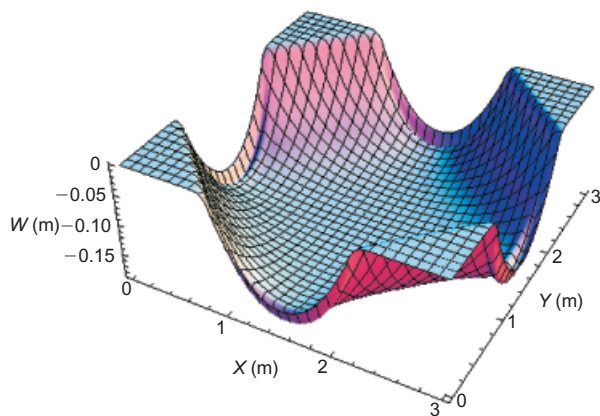


Figure 10. Vertical displacement with diamond pile caps

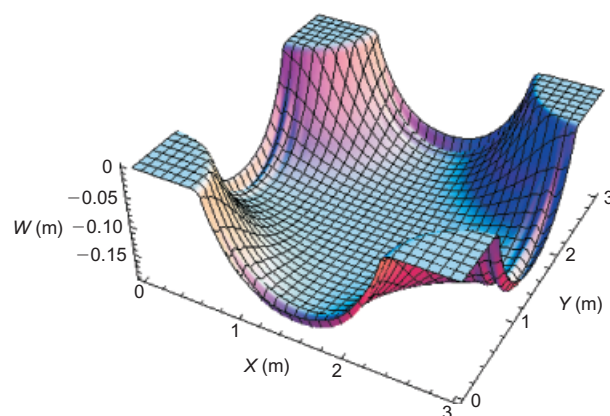


Figure 12. Vertical displacement with circular pile caps

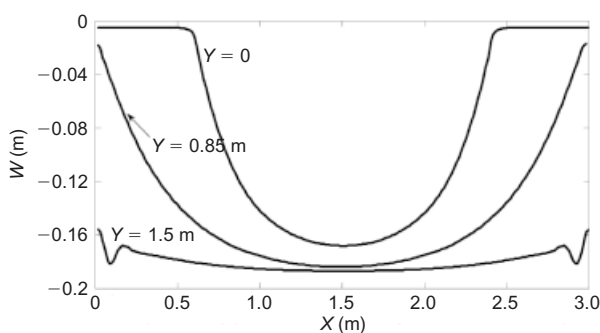


Figure 11. Vertical-displacement profiles with diamond pile caps

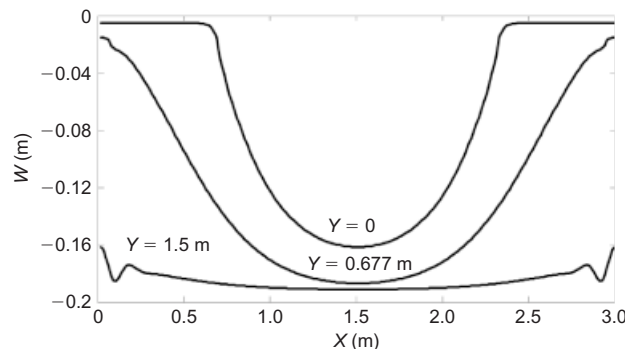


Figure 13. Vertical-displacement profiles with circular pile caps

## 7. ALTERNATIVE CASE

A similar analysis was conducted for the same pile-cap configurations and geosynthetic property values but with different embankment stresses and soil stiffnesses:  $\sigma_p = 184$  kPa (26% higher),  $\sigma_s = 24$  kPa (22% lower),  $K_p = 150$  MN/m<sup>3</sup> (414% higher), and  $K_s = 300$  kN/m<sup>3</sup> (88% higher) (Jones 2007). For this case, the stress concentration is  $n = 7.67$  and the average embankment stress is  $\sigma_{ave} = 49.6$  kPa.

The important difference from the base case is that the downward stress on the geosynthetic overlying the soft soil is lower and the stiffness of the soft soil is higher, so that the displacements will be much smaller. The ratio  $\sigma_s/K_s$ , which gives an approximate value of the maximum downward displacement, was 19.1 cm in the base case and is 8 cm here.

The results for the alternative case are summarised in Table 2. The geosynthetic exhibits a flat central region with downward displacement  $\sigma_s/K_s = 8$  cm. The slightly higher values of maximum  $W$  in Table 2 compared with  $\sigma_s/K_s$  are due to wrinkling along the edges of the unit cell. In general, the comparison of the square, diamond and circular pile caps for this case is similar to that for the base case. The maximum values of strain and stress resultant are significantly lower for the circular piles than for the diamond or square caps.

Comparing the results for the base case and the alternative case in Tables 1 and 2, the values of maximum vertical deflection, maximum horizontal deflection, maximum strain and net stress reduction ratio are all larger for the base case than for the alternative case. This occurs because the base case has a higher applied stress  $\sigma_s$  over the area underlain by soft soil, and a lower stiffness  $K_s$  of the soft soil. The larger deflection of the geosynthetic for the base case corresponds to a greater portion of the embankment load being carried by the geosynthetic, which is reflected in the larger value of the net stress reduction ratio  $SRR_{net}$ .

## 8. CONCLUDING REMARKS

Three cases were considered, involving square (Case S), diamond (Case D), and circular (Case C) pile caps at the corners of a unit cell. The geosynthetic was modelled as a thin, flexible plate with linear stress–strain response. Membrane (stretching) behaviour dominated the equilibrium shape owing to the small flexural rigidity. Partial derivatives of the displacements were approximated by finite differences, convergence studies were carried out,

and it was found to be much more effective to minimise the total energy than to solve the non-linear equilibrium equations, partly because the derivatives in the energy have lower order. Displacements and strains were computed, and stress resultants can be calculated directly from the strains.

Over the piles, the dimensional downward displacement is equal to  $\sigma_p/K_p$  (except near the edge of the pile cap), and at the centre of the unit cell it is approximately  $\sigma_s/K_s$  if  $K_s$  is not too small, where  $\sigma_p$  and  $K_p$  are the downward stress and foundation stiffness acting on the geosynthetic above the pile caps, and  $\sigma_s$  and  $K_s$  are the corresponding quantities elsewhere. The ratio  $\sigma_s/K_s$  is an upper bound on the central displacement.

Spikes occur in the strains and stresses near the edges of the pile caps, and they are particularly large near the corners in Cases S and D. Previous studies that use a cable model connecting two adjacent piles without consideration of three-dimensional effects do not uncover such strain and stress concentrations. The non-linear bending–stretching coupling used here is also important in accurately representing the behaviour of the geosynthetic.

The maximum strain  $\epsilon_x$  was compared with the strain  $\epsilon$  obtained using the same assumption as in some design methods, that the geosynthetic deflects in a parabolic shape along an edge of the unit cell (see the references cited in McGuire and Filz 2008). According to the parabolic shape assumption, the strain is computed from the cubic equation

$$96\epsilon^3 - 6K_g^2\epsilon - K_g^2 = 0 \quad \text{where} \quad K_g = \frac{\sigma_{net}A_s}{2BJ} \quad (16)$$

In Equation 16,  $\sigma_{net} = \sigma_{ave}SRR_{net}$  is the net downward stress on the geosynthetic over the soft soil (which depends on the vertical displacement obtained in the analysis, as indicated in Equation 15), and  $A_s = L^2 - 4B^2$ . For Case S, Equation 16 yields  $\epsilon = 0.0313$  for the base case and 0.0157 for the alternative case. These values are significantly lower than the maximum strains  $\epsilon_x$  of 0.0395 and 0.0240, respectively, obtained here from the three-dimensional analysis.

Further results for the cases described above are presented in Jones (2007). A cable-net model will be investigated in Part II of this study (Halvordson *et al.* 2010), and an axisymmetric model will be analysed in Part III (Plaut and Filz 2010). These papers comprise an initial investigation of 3D effects, and some basic assumptions are made, such as:

- a homogeneous, isotropic geomembrane having linear stress–strain response in Parts I and III, with a Poisson's ratio value of zero in Part I and a range of Poisson's ratio values investigated in Part III;
- a cable net with spherical joints at the nodes to model the geogrid in Part II;
- a linear foundation as a model for the soil under the geosynthetic;
- negligible friction between the geosynthetic and the soil; and
- specified uniform stresses acting downward over the

**Table 2. Maximum values and  $SRR_{net}$  for alternative case**

Case	Max $W$ (cm)	Max $U$ (cm)	Max $\epsilon_x$	$SRR_{net}$
S	8.27	0.57	0.0240	0.041
D	8.68	0.76	0.0261	0.041
C	8.47	0.58	0.0150	0.038

geosynthetic above the pile caps and between the pile caps.

The maximum strains in Part I and in most cases in Parts II and III are less than 0.04. It is recognised that geosynthetics exhibit non-linear stress–strain response. Selecting a high value of geosynthetic stiffness in analyses that employ linear stress–strain response is conservative for calculating stress concentrations when the actual geosynthetic response is strain-softening. It would be interesting to investigate the quantitative impact of non-linear response on stress concentrations.

Geosynthetic reinforcements for pile-supported embankments are often geogrids. Based on test results presented in Shinoda and Bathurst (2004), Poisson's ratio  $\nu$  is negligible for geogrids made of knitted polyester (PET), and it is very small for wide biaxial polypropylene (PP) geogrids if strains are less than 0.08–0.10. In the numerical results presented in Figures 6 and 12 of Plaut and Filz (2010), the effect of changes of  $\nu$  (in the range  $0 \leq \nu \leq 0.5$ ) on displacements, strains, and stresses is small. The value  $\nu = 0$  was used in this paper, and the behaviour should be similar for non-zero values of  $\nu$ .

The degree of inaccuracy in modelling the soil underneath the geosynthetic reinforcement layer as a distribution of independent springs is alleviated by the presence of the reinforcement, which reduces differential settlement of adjacent springs. The springs are assumed to be linear in this initial investigation, but non-linear soil models should be considered subsequently. Neglecting friction between the geosynthetic and the soil should typically lead to conservative results for stresses and strains in the geosynthetic. The impact of non-uniform stress distributions from the embankment on top of the geosynthetic in the area above the pile caps and the area between the pile caps should be investigated. Relaxation of the basic assumptions made in Parts I–III is left for future work.

## ACKNOWLEDGEMENT

This research was sponsored by the US National Science Foundation under Grant No. CMS-0408281. Any opinions, findings, and conclusions or recommendations expressed in this material are those of the authors, and do not necessarily reflect the views of the National Science Foundation. The authors are grateful to the reviewers for their helpful comments.

## NOTATIONS

Basic SI units are given in parentheses:

$A_S$	parameter in Equation 16 = $L^2 - 4B^2$ (m <sup>2</sup> )
$a_s$	area replacement ratio (dimensionless)
$B$	half-width of square or diamond pile caps (m)
$D$	flexural rigidity of geosynthetic = $Et^3/[12(1 - \nu^2)]$ (N-m)
$E$	modulus of elasticity of geosynthetic (Pa)

$E_B$	strain energy for bending of geosynthetic (N-m)
$E_{Kp}$	stored energy in soil over pile caps (N-m)
$E_{Ks}$	stored energy in soft soil (N-m)
$E_M$	strain energy for stretching of geosynthetic (N-m)
$E_T$	total energy (N-m)
$E_{\sigma p}$	potential energy for embankment stress over pile caps (N-m)
$E_{\sigma s}$	potential energy for embankment stress over soft soil (N-m)
$H$	distance between finite difference nodes (m)
$J$	in-plane stiffness of geosynthetic (N/m)
$K_g$	parameter in Equation 16 = $\sigma_{net}A_s/(2BJ)$ (dimensionless)
$K_p$	modulus of subgrade reaction under geosynthetic above pile caps (N/m <sup>3</sup> )
$K_s$	modulus of subgrade reaction for soft soil (N/m <sup>3</sup> )
$L$	centre-to-centre spacing of pile caps (m)
$m$	number of finite difference nodes along half-length between pile cap centres = $L/2H$ (dimensionless)
$n$	stress concentration ratio = $\sigma_p/\sigma_s$ (dimensionless)
$N_x, N_y, N_{xy}$	stress resultants (N/m)
$R$	radius of circular pile cap (m)
$SRR_{net}$	ratio of average net downward stress on geosynthetic in the area not supported by piles to average downward stress of embankment over unit cell (dimensionless)
$t$	thickness of geosynthetic (m)
$U, V$	in-plane displacements of geosynthetic (m)
$U_{i,j}, V_{i,j}$	values of $U, V$ at $(X, Y) = (iH, jH)$ (m)
$W$	transverse displacement of geosynthetic, positive downward (m)
$W_{i,j}$	value of $W$ at $(X, Y) = (iH, jH)$ (m)
$X, Y, Z$	coordinate axes (m)
$\epsilon$	strain in Equation 16 (dimensionless)
$\epsilon_x, \epsilon_y, \epsilon_{xy}$	strains (dimensionless)
$\nu$	Poisson's ratio (dimensionless)
$\sigma_{ave}$	average embankment stress (Pa)
$\sigma_{net}$	net downward stress on geosynthetic over soft soil (Pa)
$\sigma_p$	downward stress acting on top of geosynthetic over pile caps (Pa)
$\sigma_s$	downward stress acting on top of geosynthetic over soft soil (Pa)

## ABBREVIATIONS

C	circular pile caps
D	diamond pile caps
S	square pile caps

## REFERENCES

- Abdullah, C. H. & Edil, T. B. (2007). Behaviour of geogrid-reinforced load transfer platforms for embankment on rammed aggregate piers. *Geosynthetics International*, **14**, No. 3, 141–153.

- Abusharar, S. W., Zheng, J.-J., Chen, B.-G. & Yin, J.-H. (2008). A simplified method for analysis of a piled embankment reinforced with geosynthetics. *Geotextiles and Geomembranes*, **27**, No. 1, 39–52.
- Almeida, M. S. S., Ehrlich, M., Spotti, A. P. & Marques, M. E. S. (2007). Embankment supported on piles with biaxial geogrids. *Proceedings of the Institution of Civil Engineers: Geotechnical Engineering*, **160**, No. 4, 185–192.
- Bhandari, A., Han, J. & Wang, F. (2009). Micromechanical analysis of soil arching in geosynthetic-reinforced pile-supported embankments. *Characterization, Modeling, and Performance of Geomaterials (GSP 189)*, X. Zhang, X. Yu, J. Zhang and H. Fu, Editors, ASCE, Reston, VA, pp. 47–52.
- Camp, W. M. & Siegel, T. C. (2006). Failure of a column-supported embankment over soft ground. *Soft Soil Engineering*, D. Chan and K. T. Law, Editors, Taylor & Francis, London, pp. 117–121.
- Chen, F.-Q. & Li, A.-C. (2007). Improved design method of geosynthetic reinforced pile supported embankments on soft soil. *Chinese Journal of Geotechnical Engineering*, **29**, No. 12, 1804–1808.
- Chen, Y.-M., Cao, W.-P. & Chen, R.-P. (2008). An experimental investigation of soil arching within basal reinforced and unreinforced piled embankments. *Geotextiles and Geomembranes*, **28**, No. 2, 164–174.
- Chia, C. Y. (1980). *Nonlinear Analysis of Plates*, McGraw-Hill, New York, 422 pp.
- Collin, J. G. (2007). The use of geosynthetics to improve the performance of foundations in civil engineering. *Geosynthetics in Civil Engineering*, R. W. Sarsby, Editor, CRC Press, Boca Raton, FL, pp. 201–232.
- Filz, G. M. & Plaut, R. H. (2009). Practical implications of numerical analyses of geosynthetic reinforcement in column-supported embankments. *Advances in Ground Improvement: Research to Practice in the United States and China (GSP No. 188)*, V. R. Schaefer, M. Huang, J. Han and G. Zheng, Editors, ASCE, Reston, VA, pp. 55–62.
- Gangakhedkar, R. (2004). *Geosynthetic Reinforced Pile Supported Embankments*, ME thesis, University of Florida, Gainesville, FL, 109 pp. (<http://purl.fcla.edu/fcla/etd/UFE0004884>).
- Gharpure, A. D., Korulla, M., Jayakrishnan, P. V., Scotto, M. & Naughton, P. (2008). Design methods for pile supported basal reinforced embankments over soft clay. *Geosynthetics in Civil and Environmental Engineering*, G.-X. Li, Y.-M. Chen and X.-W. Tang, Editors, Springer, Berlin, pp. 703–708.
- Halvordson, K. A., Plaut, R. H. & Filz, G. M. (2010). Analysis of geosynthetic reinforcement in pile-supported embankments, Part II: 3D cable-net model. *Geosynthetics International*, **17**, No. 2, 68–76.
- Han, J. & Bhandari, A. (2009). Evaluation of geogrid-reinforced pile-supported embankments under cyclic loading using discrete element method. *Advances in Ground Improvement: Research to Practice in the United States and China, (GSP No. 188)*, V. R. Schaefer, M. Huang, J. Han and G. Zheng, Editors, ASCE, Reston, VA, pp. 73–82.
- Horgan, G. J. & Sarsby, R. W. (2002). The arching effect of soils over voids and piles incorporating geosynthetic reinforcement. *Proceedings of the 7th International Conference on Geosynthetics*, P. Delmas, J. P. Gourc and H. Girard, Editors, Swets & Zeitlinger, Lisse, The Netherlands, Vol. 1, pp. 373–378.
- Huang, J. & Han, J. (2009). 3D coupled mechanical and hydraulic modeling of a geosynthetic-reinforced deep mixed column-supported embankment. *Geotextiles and Geomembranes*, **27**, No. 4, 272–280.
- Huang, J., Han, J. & Oztoprak, S. (2009). Coupled mechanical and hydraulic modeling of geosynthetic-reinforced column-supported embankments. *Journal of Geotechnical and Geoenvironmental Engineering*, **135**, No. 8, 1011–1021.
- Jenck, O., Dias, D. & Kastner, R. (2005). Soft ground improvement by vertical rigid piles: two-dimensional physical modelling and comparison with current design methods. *Soils and Foundations*, **45**, No. 6, 15–30.
- Jenck, O., Dias, D. & Kastner, R. (2007). Two-dimensional physical and numerical modeling of a pile-supported earth platform over soft soil. *Journal of Geotechnical and Geoenvironmental Engineering*, **133**, No. 3, 295–305.
- Jones, B. M. (2007). *Three-Dimensional Finite Difference Analysis of Geosynthetic Reinforcement Used in Column-Supported Embankments*, MS thesis, Virginia Polytechnic Institute and State University, Blacksburg, VA, 213 pp. (<http://scholar.lib.vt.edu/theses/available/etd-12112007-190833/>).
- Kempfert, H.-G. & Gebreselassie, B. (2006). *Excavations and Foundations in Soft Soils*, Springer-Verlag, Berlin, 576 pp.
- Liu, H. L., Ng, C. W. W. & Fei, K. (2007). Performance of a geogrid-reinforced and pile-supported highway embankment over soft clay: case study. *Journal of Geotechnical and Geoenvironmental Engineering*, **133**, No. 12, 1483–1493.
- Love, J. & Milligan, G. (2003). Design methods for basally reinforced pile-supported embankments over soft ground. *Ground Engineering*, **36**, No. 3, 39–43.
- McGuire, M. P. & Filz, G. M. (2008). Quantitative comparison of theories for geosynthetic reinforcement of column-supported embankments. *Proceedings of the First Pan American Geosynthetics Conference and Exhibition*, Cancun, Mexico, March 2008, 10 pp.
- McGuire, M. P., Filz, G. M. & Almeida, M. S. S. (2009). Load-displacement compatibility analysis of a low-height column-supported embankment. *Contemporary Topics in Ground Modification, Problem Soils, and Geo-Support (GSP No. 187)*, M. Iskander, D. F. Laefer and M. H. Hussein, Editors, ASCE, Reston, VA, pp. 225–232.
- Oh, Y. I. & Shin, E. C. (2007). Reinforcement and arching effect of geogrid-reinforced and pile-supported embankment on marine soft ground. *Marine Georesources and Geotechnology*, **25**, No. 2, 97–118.
- Plaut, R. H. & Filz, G. M. (2010). Analysis of geosynthetic reinforcement in pile-supported embankments, Part III: Axisymmetric model. *Geosynthetics International*, **17**, No. 2, 77–85.
- Shinoda, M. & Bathurst, R. J. (2004). Lateral and axial deformation of PP, HDPE and PET geogrids under tensile load. *Geotextiles and Geomembranes*, **22**, No. 4, 205–222.
- Smith, M. E. (2005). *Design of Bridging Layers in Geosynthetic-Reinforced Column-Supported Embankments*, PhD thesis, Virginia Polytechnic Institute and State University, Blacksburg, VA, 235 pp.
- Smith, M. & Filz, G. (2007). Axisymmetric numerical modeling of a unit cell in geosynthetic-reinforced, column-supported embankments. *Geosynthetics International*, **14**, No. 1, 1–10.
- Szilar, R. (2004). *Theories and Applications of Plate Analysis: Classical, Numerical, and Engineering Methods*, Wiley, Hoboken, NJ, 1,024 pp.
- Timoshenko, S. P. & Woinowsky-Krieger, S. (1959). *Theory of Plates and Shells*, 2nd edition, McGraw-Hill, New York, 580 pp.
- Van Eekelen, S. J. M. & Bezuijen, A. (2008). Design of piled embankments considering the basic starting points of the British Standard BS8006. *EuroGeo4: 4th European Geosynthetics Conference*, Paper No. 315.
- Van Eekelen, S., Bezuijen, A. & Alexiew, D. (2008). Piled embankments in the Netherlands, a full-scale test, comparing 2 years of measurements with design calculations. *EuroGeo4: 4th European Geosynthetics Conference*, Paper No. 264.
- Wolfram, S. (2003). *The Mathematica Book*, 5th edition, Wolfram Media, Champaign, IL, 1,488 pp.
- Zhang, L., Zhao, M.-H. & He, W. (2007). Working mechanism of two-direction reinforced composite foundation. *Journal of Central South University of Technology*, **14**, No. 4, 589–594.
- Zheng, J.-J., Chen, B.-G., Lu, Y.-E., Abusharar, S. W. & Yin, J.-H. (2009). The performance of an embankment on soft ground reinforced with geosynthetics and pile walls. *Geosynthetics International*, **16**, No. 3, 173–182.

The Editor welcomes discussion on all papers published in *Geosynthetics International*. Please email your contribution to [discussion@geosynthetics-international.com](mailto:discussion@geosynthetics-international.com) by 15 October 2010.